

## The Effect of Stokes Drift and Transient Rip Currents on the Inner Shelf. Part I: No Stratification

NIRNIMESH KUMAR

*University of Washington, Seattle, Washington*

FALK FEDDERSEN

*Scripps Institution of Oceanography, La Jolla, California*

(Manuscript received 29 March 2016, in final form 17 November 2016)

### ABSTRACT

This is part one of a two-part study focused on Stokes drift and transient rip current (TRC) effects on the unstratified (this paper) and stratified (see Part II) inner shelf. A TRC-generating, wave-resolving model *funwaveC* is coupled to the 3D, wave-averaged wave and circulation model Coupled Ocean–Atmosphere–Wave–Sediment Transport (COAWST). Two simulations (R1 and R2) are performed on an unstratified inner shelf and surfzone with typical bathymetry and wave conditions. R1 is a COAWST-only simulation (no TRCs), while R2 has *funwaveC*–COAWST coupling (with TRCs). R2 and *funwaveC* vertical vorticity (eddy) statistics are similar, indicating that the model coupling accurately generates TRCs, with TRC-induced eddies out to four surfzone widths offshore. R1 has a two-layered, inner-shelf-to-surfzone-connected, mean Lagrangian circulation, while R2 has separate inner shelf and surfzone circulation cells. The R2, TRC-induced, cross-shore and vertical eddy velocities are stronger than the R1 or R2 mean Lagrangian velocity out to four surfzone widths offshore. The R2, inner-shelf, mean, vertical eddy diffusivity is an order of magnitude larger than R1 out to four surfzone widths offshore. Both R1 and R2 are in a Stokes–Coriolis balance at six surfzone widths offshore, as is R1 at three surfzone widths offshore. For R2, TRC-induced horizontal advection and vertical mixing dominate the cross-shore momentum dynamics at three surfzone widths offshore. The R2 surfzone and inner-shelf cross-shore exchange velocity is 2–10 times larger for R1 because of the TRC-induced stirring. Accurate, unstratified, inner-shelf simulations of pollution, larval, or sediment transport must include transient rip currents. In Part II, the effects of Stokes drift and TRCs on the stratified inner shelf are examined.

### 1. Introduction

The nearshore (the  $\approx 1$  km of the ocean, adjacent to the shoreline) is the transition region from land to the ocean consisting of the surfzone (from the shoreline to the seaward extent of depth-limited breaking  $L_{SZ}$ ) and the inner shelf (from  $L_{SZ}$  to  $\approx 15$ -m water depths). Nearshore water quality is often compromised by pathogens, human viruses, and excessive nutrient supply from terrestrial runoff (Halpern et al. 2008; Boehm et al. 2017). The nearshore is also critical for intertidal ecosystems as benthic invertebrate larvae must transition

this region (e.g., Pineda et al. 2007; Shanks et al. 2010; Fujimura et al. 2014). Cross-shelf exchange of nearshore tracers (e.g., pathogens, contaminants, nutrients, larvae, sediment, and heat) is three-dimensional, complex, and driven by a variety of processes, including surface gravity waves through Stokes drift and rip currents.

Surface waves propagating toward the shoreline have a net mass flux (Stokes drift). On an alongshore, uniform bathymetry, the mean, depth-integrated, cross-shore mass flux must be zero. Thus, the depth-integrated, on-shore Stokes drift  $\bar{u}_{st}$  balances the depth-integrated, off-shore-directed, mean Eulerian velocity  $\bar{u}_e$ :

$$\int_{-h}^{\bar{\eta}} \bar{u}_e(z) dz = - \int_{-h}^{\bar{\eta}} \bar{u}_{st}(z) dz, \quad (1)$$

where  $z$  is the vertical coordinate,  $h$  is the still water depth, and  $\bar{\eta}$  is the mean sea surface. However, across the surfzone and inner shelf,  $\bar{u}_e(z)$  and  $\bar{u}_{st}(z)$  do not

 Denotes content that is immediately available upon publication as open access.

Corresponding author e-mail: N. Kumar, nirni@uw.edu

necessarily balance at any particular depth (e.g., Haines and Sallenger 1994; Garcez Faria et al. 2000; Reniers et al. 2004b; Lentz et al. 2008; Fewings et al. 2008; Kumar et al. 2012; Özkan Haller 2014). The resulting nonzero cross-shore Lagrangian velocity  $\bar{u}_L(z) = \bar{u}_e(z) + \bar{u}_{st}(z)$  leads to a two-dimensional (2D), mean Lagrangian overturning circulation and to cross-shelf exchange (e.g., Lentz and Fewings 2012).

Surfzone and inner-shelf cross-shore exchange is also induced by horizontal eddies. On an alongshore, uniform bathymetry, surfzone cross-shore exchange is dominated by surfzone eddies over the mean Lagrangian velocity  $\bar{u}_L(z)$  in both dye and drifter observations (Spydell et al. 2007, 2009; Clark et al. 2010) and 2D, horizontal, wave-resolving modeling (Spydell and Feddersen 2009; Clark et al. 2011). The surfzone eddies are generated by finite-crest-length breaking waves (Peregrine 1998; Johnson and Pattiaratchi 2006; Clark et al. 2012; Feddersen 2014). The surfzone is also observed to be vertically well mixed (Hally-Rosendahl et al. 2014, 2015) due to strong breaking wave-driven turbulence (e.g., Feddersen 2012). Tracer exchange between the surfzone and inner shelf is dominated by transient (Hally-Rosendahl et al. 2014, 2015; Hally-Rosendahl and Feddersen 2016), or bathymetrically controlled (Reniers et al. 2009; Brown et al. 2015), rip currents over nonzero  $\bar{u}_L(z)$ . Bathymetrically controlled rip currents occur at fixed, alongshore locations or on rip-channeled beaches and are a component of the mean circulation (e.g., MacMahan et al. 2006; Dalrymple et al. 2011). In contrast, transient rip currents (TRCs) result from surfzone eddy coalescence (Johnson and Pattiaratchi 2006), are episodic, and are analogous to two-dimensional turbulence (Feddersen 2014). Unlike bathymetrically controlled rip currents, TRCs can occur on alongshore, uniform beaches and can have short (10–50 m), alongshore length scales (Hally-Rosendahl et al. 2014, 2015).

On the alongshore-uniform inner shelf, mass conservation (1) must also hold (e.g., Lentz et al. 2008; Kirincich et al. 2009). For idealized steady and unstratified conditions with weak winds and weak mixing, the Stokes–Coriolis force drives an inner-shelf Eulerian return flow that identically balances (denoted Stokes–Coriolis balance; Xu and Bowen 1994; Lentz et al. 2008)

$$f\bar{u}_e(z) = -f\bar{u}_{st}(z), \quad (2)$$

where  $f$  is the Coriolis frequency. The Stokes–Coriolis balance results in zero-mean Lagrangian flow  $\bar{u}_L = \bar{u}_e + \bar{u}_{st} = 0$  and zero cross-shelf exchange. For subtidally ( $>33$ -h time scale) averaged Eulerian cross-shelf velocities, weak winds, and unstratified conditions,

an approximate Stokes–Coriolis balance [(2)] in  $h = 12$ -m depth was observed through significant bin averaging (Lentz et al. 2008). Modeled inner-shelf eddies induced by TRCs can lead to cross-shelf exchange that is larger than an estimated Stokes drift–driven exchange up to two to five surfzone widths  $L_{SZ}$  offshore of the shoreline (Suanda and Feddersen 2015). However, this model was 2D and did not resolve the vertical. The vertical structure of the inner-shelf eddy field, its interaction with the Lagrangian overturning circulation, and its role in vertical mixing and cross-shore exchange on an unstratified inner shelf is not understood.

In addition, the inner shelf is often stratified, which can influence cross-shelf exchange. Stratification can be strong to within 80 m of the surfzone, strongly inhibiting vertical tracer mixing (Hally-Rosendahl et al. 2014). At subtidal ( $\geq 33$  hr) time scales, stronger stratification together with along- or cross-shelf winds modifies the exchange across the inner to outer shelf in observations and models (e.g., Allen et al. 1995; Lentz 2001; Kirincich et al. 2005; Austin and Lentz 2002; Fewings et al. 2008; Tilburg 2003; Horwitz and Lentz 2014). For weak winds, the stratified inner shelf, with presumably weaker vertical mixing, was found to deviate from a Stokes–Coriolis balance (Lentz et al. 2008), resulting in enhanced exchange.

Three-dimensional (3D) TRCs on either an unstratified or stratified inner shelf have never before been modeled. The ability to accurately model 3D TRCs from a well-mixed surfzone across an inner shelf is required to diagnose cross-shelf exchange mechanisms. A wave-resolving model is needed to simulate surfzone eddies, their coalescence, and the resulting TRCs that eject out onto the inner shelf. However, wave-resolving Boussinesq models such as funwaveC are essentially depth integrated and do not resolve vertical variations in velocity or stratification, potentially important to inner-shelf exchange. In contrast, the coupled ocean circulation and wave propagation model Coupled Ocean–Atmosphere–Wave–Sediment Transport (COAWST) include Stokes drift, Coriolis, and the vertically varying circulation and stratification (e.g., Kumar et al. 2012). However, the wave-averaged COAWST does not include the finite-crest-length, wave-breaking, surfzone, eddy generation mechanism. Unlike other 3D nearshore models (Reniers et al. 2009), COAWST also does not include wave group forcing, which could create larger-scale (many hundreds of meters) TRCs, which is a small component of TRC forcing (Feddersen 2014). Thus, in order to investigate the effects of TRCs on the inner shelf, the two models must be coupled.

In this two-part study, a funwaveC–COAWST coupling method is developed to allow TRC effects on

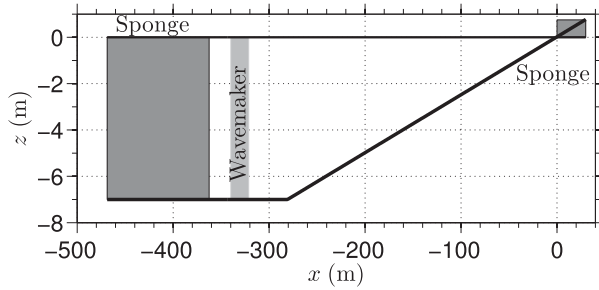


FIG. 1. The funwaveC schematic showing model bathymetry  $h(x)$ , sponge layers, and wavemaker regions vs cross-shore coordinate  $x$ , where  $x = 0$  m is the still-water shoreline. Sponge layers (dark shaded regions) are located at the ends of the model domain. The wave maker (light shaded region) radiates waves onshore and offshore.

an unstratified (Part I, this manuscript) and stratified (Kumar and Feddersen 2016, hereinafter Part II) inner shelf to be explored. In Part I, the funwaveC–COAWST coupling method is developed where funwaveC surfzone eddy forcing is extracted and prescribed as a body force to COAWST (section 2) and tested by comparing vorticity statistics (section 3). Two simulations with typical bathymetry and waves without winds are analyzed, one without (R1) and one with (R2) TRC effects. The effects of TRCs on the inner-shelf mean Lagrangian overturning streamfunction, eddy variability, and mean vertical eddy viscosity are examined (section 4). The discussion (section 5) examines mean cross-shore momentum balances and cross-shore exchange velocity and the effects of TRCs. The results are summarized in section 6. In Part II, constant initial stratification is included in the simulations without and with TRC effects, the effects of TRCs on a stratified inner shelf are examined in detail.

## 2. Methods

### a. The funwaveC model and configuration

The open-source, wave-resolving, Boussinesq model funwaveC has been extensively used to study surfzone drifter and tracer dispersion, surfzone eddies, and shoreline runup (e.g., Spydell and Feddersen 2009; Feddersen et al. 2011; Clark et al. 2011; Guza and Feddersen 2012; Feddersen 2014). It has also been used to study transient rip current ejections of eddies and tracer onto the inner shelf (Suanda and Feddersen 2015; Hally-Rosendahl and Feddersen 2016). The time-dependent Nwogu (1993) model equations are similar to the nonlinear, shallow-water equations and include higher-order dispersive terms. Model details are found elsewhere (Feddersen et al. 2011). Relevant to coupling with the wave-averaged COAWST model, the horizontal momentum equation for horizontal velocity  $\mathbf{u}$  is

$$\frac{\partial \mathbf{u}}{\partial t} + \mathbf{u} \cdot \nabla \mathbf{u} = -g \nabla \eta + \mathbf{F}_d + \mathbf{F}_{br} - \frac{\tau_b}{(\eta + h)} - \mu_{bi} \nabla^4 \mathbf{u}, \quad (3)$$

where  $g$  is the gravity,  $\eta$  is the free surface,  $\mathbf{F}_d$  is the dispersive term (Nwogu 1993),  $\mathbf{F}_{br}$  is the breaking term, and  $\tau_b$  is the instantaneous bottom stress given by a quadratic drag law

$$\tau_b = C_d |\mathbf{u}| \mathbf{u}, \quad (4)$$

with the uniform drag coefficient  $C_d = 2.3 \times 10^{-3}$  (Spydell and Feddersen 2009; Feddersen et al. 2011). Note that the time-averaged bottom stress will include the effect of waves. The biharmonic friction  $\nabla^4 \mathbf{u}$  term damps instabilities with a hyperviscosity  $\mu_{bi} = 0.4 \text{ m}^4 \text{ s}^{-1}$ . The breaking wave forcing is parameterized as a Newtonian damping (Kennedy et al. 2000), where

$$\mathbf{F}_{br} = (h + \eta)^{-1} \nabla \cdot [\nu_{br} (h + \eta) \nabla \mathbf{u}], \quad (5)$$

with the Lynett (2006) eddy viscosity  $\nu_{br}$ . Note that  $\mathbf{F}_{br}$  has both irrotational and rotational  $\mathbf{F}_{br}^{(rot)}$  components.

In wave-resolving Boussinesq models, horizontal surfzone eddies (vertical vorticity  $\omega$ ) are generated by the rotational component of the wave-breaking force  $\mathbf{F}_{br}$  such that

$$\frac{\partial \omega}{\partial t} = \dots + \nabla \times \mathbf{F}_{br}. \quad (6)$$

On an alongshore, uniform bathymetry, nonzero  $\nabla \times \mathbf{F}_{br}$  is generated with a finite-crest-length breaking of a directionally spread wave field. Thus, a wave-resolving Boussinesq model is necessary to drive surfzone eddies and simulate the effect of transient rip currents. However, funwaveC does not resolve vertical density or velocity structure.

The model funwaveC is used to simulate transient rip currents due to normally incident random directional waves on an alongshore, uniform bathymetric setup (Fig. 1). The funwaveC alongshore-uniform bathymetry is cross-shore ( $x$ ) planar with a slope of 0.025 to a water depth of  $h = 7$  m at  $x = -280$  m (Fig. 1). Farther offshore ( $-470 < x < -280$  m) the water depth is constant at  $h = 7$  m. The total cross-shore domain length is 500 m with grid size  $\Delta x = 1.25$  m, while the alongshore domain is 1000 m with  $\Delta y = 1$  m. The alongshore boundary conditions are periodic. A 105-m-wide sponge layer is located at the offshore model boundary absorbing outgoing wave energy. A 30-m-wide sponge layer is applied at the onshore boundary absorbing shoreline wave energy (Fig. 1). A 20-m-wide source function wavemaker (Wei et al. 1999; Suanda et al. 2016) located at  $x = -330$  m (light, shaded region Fig. 1) generates

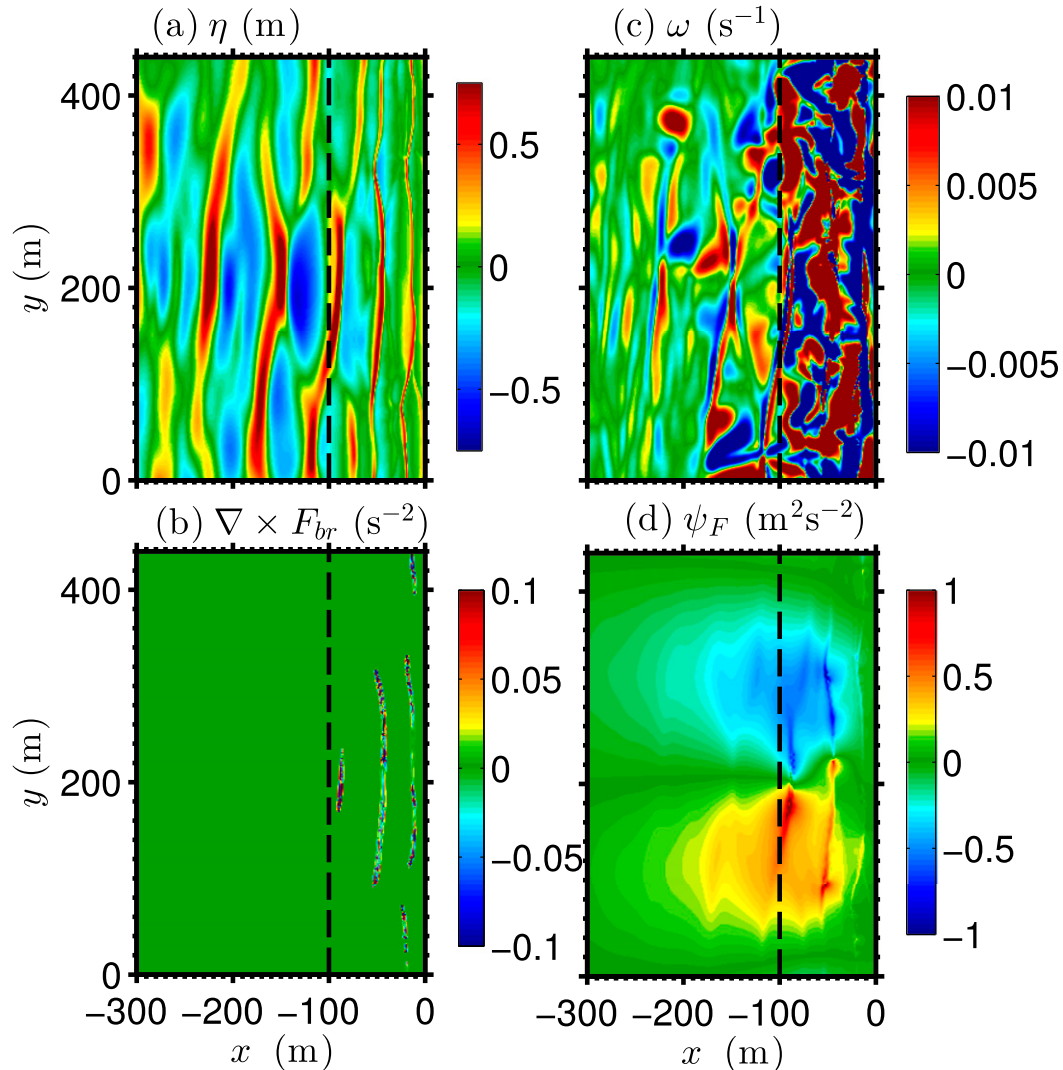


FIG. 2. The funwaveC-modeled snapshots of (a) sea surface elevation  $\eta$ , (b) curl of wave-breaking force  $\nabla \times \mathbf{F}_{br}$ , (c) vertical vorticity  $\omega$ , and (d) forcing streamfunction  $\psi_F$  (7).

random, normally incident, directionally spread JONSWAP frequency spectrum with significant wave height  $H_s = 1$  m, peak period  $T_p = 10$  s, bulk (mean) wave angle  $\theta = 0^\circ$ , and directional spread  $\sigma_\theta = 10^\circ$ . This directional wave field allows vorticity generation due to finite-crested wave breaking (Peregrine 1998). The funwaveC  $\eta$  and  $\mathbf{u}$  initial conditions are zero. Model simulation is conducted for 12 h, and model variables are output at 1 Hz.

In the funwaveC simulation, random, directionally incident waves propagate shoreward, shoal, begin breaking near  $x = -L_{SZ}$ , where  $L_{SZ} = 100$  m is the nominal surfzone width, and dissipate as they approach the shoreline (Fig. 2a). The directionally spread wave field results in finite-crested wave breaking. Within the surfzone ( $x > -L_{SZ}$ ), this generates nonzero curl of

breaking wave forcing  $\nabla \times \mathbf{F}_{br}$  up to  $0.1 \text{ s}^{-2}$  (Fig. 2c) that generates a rich surfzone vertical vorticity (eddies) field on a variety of length scales (Fig. 2b). Shorter eddies coalesce to larger scales (Spydell and Feddersen 2009; Feddersen 2014) and create episodic, transient rip currents (e.g., Johnson and Pattiaratchi 2006; Suanda and Feddersen 2015) that eject eddies (vorticity) onto the inner shelf.

Surfzone eddy forcing is isolated from wave-resolving funwaveC for use within the wave-averaged COAWST. The rotational component of  $\mathbf{F}_{br}$  generating the surfzone eddies can be compactly represented with a scalar forcing streamfunction  $\psi_F$ , representing the vorticity generation due to breaking of finite-crested waves:

$$\nabla \times \mathbf{F}_{br} = \nabla^2 \psi_F, \quad (7)$$

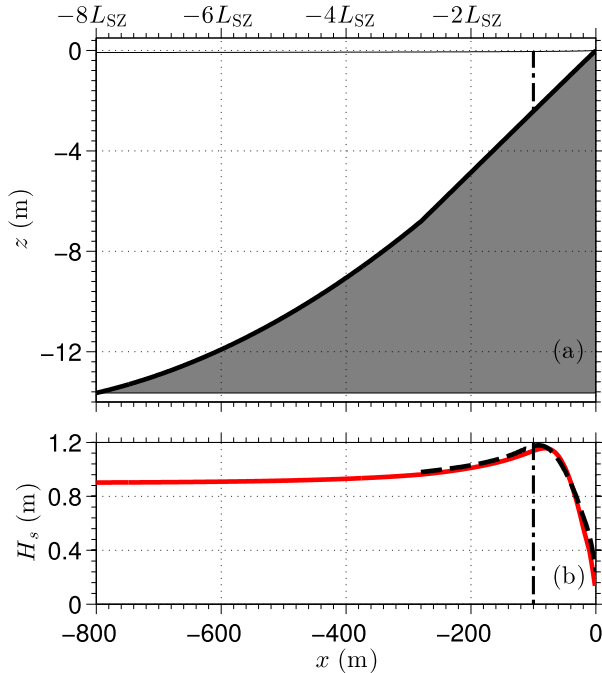


FIG. 3. (a) COAWST cross-shore bathymetry (solid black line) and (b) significant wave height  $H_s$  for SWAN (red) and funwaveC (black dashed). In (a) and (b), the vertical dashed-dotted line delimits the surfzone  $x = -L_{SZ}$  (where  $L_{SZ} = 100$  m).

which is solved (e.g., Spydell and Feddersen 2009) at each time step (Fig. 2d) and stored for input to COAWST (section 2b). An example  $\psi_F$  has a dipole with higher magnitude within the surfzone ( $x > -L_{SZ}$ ), decreasing on the inner shelf (as in Fig. 2d). Much of the nonzero  $\psi_F$  has  $\nabla^2\psi_F = 0$  and does not force vorticity in Fig. 2c. However, each monopole has localized maxima at the locations where instantaneous wave breaking corresponds to vorticity forcing (Fig. 2d).

### b. COAWST model and configuration

The open-source COAWST modeling system (Warner et al. 2010) here couples the Simulating Waves Nearshore (SWAN) wave model and the ROMS circulation model. SWAN (Booij et al. 1999; Ris et al. 1999) includes wave shoaling, refraction, and depth-limited breaking. The Regional Ocean Modeling System (ROMS) is a 3D ocean circulation model solving the wave-averaged Navier–Stokes equations with the hydrostatic and Boussinesq approximations (Shchepetkin and McWilliams 2005; Haidvogel et al. 2008; Shchepetkin and McWilliams 2009). Wave–current interaction is based on the vortex force formalism ( Craik and Leibovich 1976), separating conservative (McWilliams et al. 2004) and nonconservative (breaking wave–induced forcing) wave effects (Uchiyama et al. 2010; Kumar et al. 2012). COAWST has been validated and used in variety of

surfzone, tidal inlet, inner-shelf, and midshelf applications (Kumar et al. 2011, 2012; Olabarrieta et al. 2011; Feddersen et al. 2016; Kumar et al. 2015, 2016). However, COAWST is wave averaged and cannot generate surfzone eddies via finite-crested wave breaking. Therefore, transient rip currents are not generated and surfzone and inner-shelf eddy fields will be inaccurate, motivating the coupling with the wave-resolving funwaveC.

The COAWST model is set up with similar bathymetry and waves as funwaveC. The COAWST parameter setup follows Kumar et al. (2012), validated with Duck94 observations. The COAWST model domain (both SWAN and ROMS) is alongshore uniform with a cross-shore width of 800 m and alongshore length of 1000 m. The cross-shore and alongshore grid resolution are 1.25 and 2 m, respectively. Alongshore periodic boundary conditions are used. The cross-shore bathymetric profile  $h(x)$  matches the planar funwaveC bathymetry for  $x > -280$  m (thick black line; Fig. 3a). Farther offshore the bathymetry is concave and the slope reduces typical to inner-shelf bathymetry profiles in Southern California (Kumar et al. 2015).

At the SWAN offshore boundary (i.e.,  $x = -800$  m;  $h = 14$  m), a normally incident directionally spread wave field is applied ( $H_s = 0.95$  m, peak period  $T_p = 10$  s, mean wave direction  $\bar{\theta} = 0^\circ$ , and a directional spread  $\sigma_\theta = 10^\circ$ ). SWAN cross shore transforms the frequency–directional spectra with standard parameters. The SWAN incident wave field is set so that for  $h \geq 7$  m the SWAN and funwaveC  $H_s$  match. Here, SWAN is one-way coupled to ROMS, allowing for periodic SWAN boundary conditions. Waves are constant for the 24-h simulation period. The wave forcing from SWAN is irrotational and generates wave-driven setdown and setup. SWAN is also used to derive other bulk parameters, most importantly the vertically varying Stokes drift  $\bar{u}_{st}(z)$ .

The ROMS onshore boundary (i.e.,  $x = 0$ ) is closed for all prognostic variables. At the offshore boundary ( $x = -800$  m) the vertically varying cross-shore Eulerian velocity is set to anti-Stokes flow  $u_e = -\bar{u}_{st}$ , such that the offshore boundary mass flux is zero. At the offshore boundary, the alongshore velocity and the sea surface elevation are set to zero. ROMS uses 10 bathymetry-following vertical levels. The model simulation is conducted for 24 h with a ROMS baroclinic time step of 0.25 s and barotropic time step of 0.0125 s. Earth’s rotation effect is included with the Coriolis parameter  $f = 8.09 \times 10^{-5} \text{ s}^{-1}$ , typical of Southern California. To generate surfzone eddies within COAWST, the funwaveC-derived rotational wave forcing, that is,

$$\mathbf{F}_{br}^{(rot)} = \nabla \times \psi_F(x, y, t) \hat{\mathbf{k}}, \quad (8)$$

where  $\hat{\mathbf{k}}$  is the unit upward vector, is prescribed as a ROMS depth-uniform body force every 1 s, which ROMS interpolates in time. Waves can propagate multiple grid points over the 1-s forcing update period, particularly in the outer surfzone. This can lead to aliasing of the rotational wave forcing, which is discussed in section 3b. Note that only the rotational component of funwaveC wave forcing is passed to ROMS, and the irrotational component (leading to setup) is not included. This rotational force  $\mathbf{F}_{\text{br}}^{(\text{rot})}$  has zero mean. As the funwaveC simulation was for 12 h, the ROMS body force is symmetric from 1–12 to 12–24 h. The rate of work ( $\langle \mathbf{F}_{\text{br}}^{(\text{rot})} \cdot \mathbf{u} \rangle$  (where  $\langle \cdot \rangle$  denotes the mean) associated with eddy generation is expected to be small as the local velocity dynamics are  $\partial \mathbf{u} / \partial t \approx \mathbf{F}_{\text{br}}^{(\text{rot})}$  (e.g., Long and Özkan-Haller 2009), and with zero-mean  $\mathbf{F}_{\text{br}}^{(\text{rot})}$ ,  $\mathbf{u}$  and  $\mathbf{F}_{\text{br}}^{(\text{rot})}$  are principally in quadrature. The mean, cross-shore, integrated rate of work  $\int_{-L_{\text{SZ}}}^0 \langle \mathbf{F}_{\text{br}}^{(\text{rot})} \cdot \mathbf{u} \rangle dx$  is  $< 0.5\%$  of the incident cross-shore wave energy flux, confirming this expectation and demonstrating that this model coupling is consistent in its partition of incident wave energy flux. ROMS bottom stress uses a quadratic drag law with uniform drag coefficient  $C_d = 0.0025$  but does not include wave effects.

Vertical eddy viscosity  $K_v$  is given by a  $k$ - $\epsilon$  turbulence closure model that solves transport equations for turbulent kinetic energy  $k$  and turbulent dissipation  $\epsilon$  (e.g., Warner et al. 2005; Feddersen and Trowbridge 2005). Near bed, the model assumes a production and dissipation balance with bottom roughness  $z_{\text{ob}} = 0.001$  m; 5% of the SWAN wave dissipation (Feddersen 2012) is provided as a TKE surface flux (Kumar et al. 2012). ROMS lateral eddy viscosity is elevated in the surfzone ( $K_H = 0.2 \text{ m}^2 \text{ s}^{-1}$  near shoreline), consistent with the background diffusivities previously used in nearshore tracer wave-resolving model studies (Clark et al. 2011; Hally-Rosendahl and Feddersen 2016), and decays offshore to  $K_H = 0.01 \text{ m}^2 \text{ s}^{-1}$  seaward of the surfzone. Other COAWST parameters are identical to those used in Kumar et al. (2012).

The funwaveC and SWAN  $H_s(x)$  are compared to ensure the models are representing similar wave fields (Fig. 3b). The offshore SWAN  $H_s = 0.95$  m shoals to  $H_s = 1.2$  m near the breakpoint  $x = -100$  m and decays toward the shoreline (black dashed, Fig. 3b). The funwaveC and SWAN modeled  $H_s$  agree very well with differences of 1–2 cm (black dashed and gray in Fig. 3b), indicating that cross-shore wave energy fluxes and breaking wave dissipation are consistent in both models.

### c. COAWST simulations R1 and R2: Without and with transient rip currents

Here, in Part I, two, nearly identical, vertically resolving COAWST simulations (denoted R1 and R2) are

performed. Both simulations are unstratified. The only difference is that R1 does not have the rotational surfzone eddy forcing  $\mathbf{F}_{\text{br}}$  [(8)] derived from funwaveC, whereas R2 does include funwaveC-derived  $\mathbf{F}_{\text{br}}$ . Thus, R2 will have transient rip currents ejecting onto the inner shelf, whereas R1 does not have transient rip currents. In Part II, two additional simulations R3 and R4 are performed that are identical to R1 and R2, respectively, but include a constant stratification initial condition.

### 3. Comparison of R2 and funwaveC vorticity

Prior to examining the effects of surfzone eddy generation on the unstratified (Part I) and stratified (Part II) inner shelf, the R2-simulated surfzone vorticity is compared to that of funwaveC. R2 vertical vorticity is examined to determine if funwaveC–COAWST coupling leads to TRCs that eject onto the inner shelf (Fig. 4) in a manner qualitatively consistent with funwaveC. At 1 h (0 h is model start time), surfzone ( $x > -L_{\text{SZ}}$ , where surfzone width  $L_{\text{SZ}} = 100$  m) vorticity structure is rich (Fig. 4a) and variable, qualitatively similar in magnitude and length scales to wave-resolving (funwaveC), model-simulated vorticity (e.g., Feddersen 2014; Suanda and Feddersen 2015). At later times, surfzone vorticity is similar (Figs. 4b,c) as surfzone root-mean-square vorticity typically equilibrates in under an hour (Feddersen et al. 2011). The small effect of the aliased wave forcing can be seen in the 4–5-m vorticity finestructure in the outer surfzone. At 1 h, surfzone eddies are ejected as TRCs onto the inner shelf out to  $2.5L_{\text{SZ}}$ . Later, at 12 h, the R2 inner-shelf eddy field is stronger and vorticity variability (monopoles, dipoles, and filaments) occurs up to  $4.5L_{\text{SZ}}$  (Fig. 4b). Inner-shelf vorticity has a broad range of length scales (50–100 m) with a magnitude of  $10^{-2} \text{ s}^{-1}$ , approximately two orders of magnitude stronger than the Coriolis term  $f$ . At 24 h, the inner-shelf eddy field is similar to the eddy field at 12 h (Figs. 4b,c), indicating an equilibrated, inner-shelf eddy field. Inner-shelf ( $-5L_{\text{SZ}} < x < -L_{\text{SZ}}$  m), integrated square vorticity equilibrates at 6 h (not shown). These R2 TRCs and inner-shelf eddy structure are qualitatively similar to observed (Marmorino et al. 2013; Hally-Rosendahl et al. 2014, 2015) and funwaveC-modeled TRCs (Suanda and Feddersen 2015; Hally-Rosendahl and Feddersen 2016), indicating that the funwaveC–COAWST coupling works well.

Next, funwaveC and R2 vorticity  $\omega$  statistics are compared. First, funwaveC and R2 cross-shore profiles of root-mean-square vorticity  $\text{RMS}(\omega)$  are estimated over 6–12 h. The depth-averaged vorticity is used for R2. As both funwaveC and R2 mean Eulerian currents are

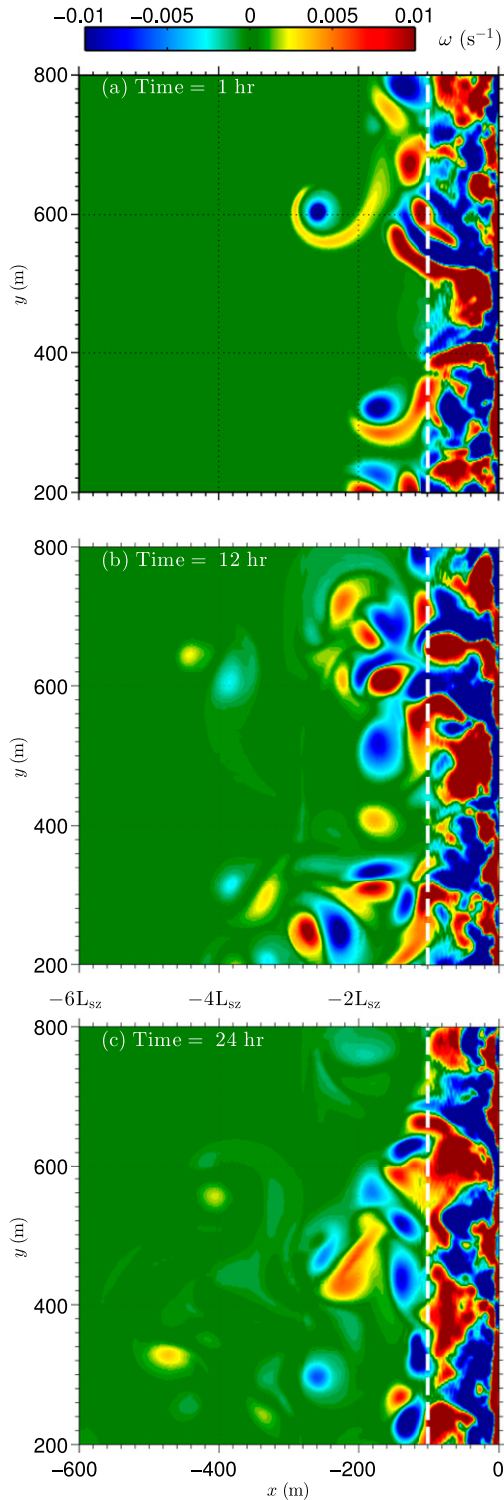


FIG. 4. R2 (with TRCs) surface vertical vorticity  $\omega$  at times (a) 1, (b) 12, and (c) 24 h. The dashed line delimits the surfzone  $x = -L_{SZ}$ .

near zero,  $RMS(\omega)$  and standard deviation of  $\omega$  are essentially identical. R2 and funwaveC  $RMS(\omega)$  are similar from near shoreline ( $x = 0$  m) to  $x = -3L_{SZ}$  offshore (Fig. 5a). At midsurfzone ( $x = -L_{SZ}/2$ ), funwaveC  $RMS(\omega) = 0.025 \text{ s}^{-1}$  and decays quasi exponentially to  $\approx 0.5 \times 10^{-3} \text{ s}^{-1}$  at  $x = -3L_{SZ}$  (solid black, Fig. 5a). The R2  $RMS(\omega)$  is similar to funwaveC particularly from midsurfzone and farther offshore (red, Fig. 5a), although the offshore decay is slightly weaker with R2  $RMS(\omega) \approx 10^{-3} \text{ s}^{-1}$  at  $x = -3L_{SZ}$ .

Next, the alongshore wavenumber spectra of vorticity  $S_{\omega\omega}(k_y)$  from funwaveC and R2 are compared at the surfzone/inner-shelf boundary  $x = -L_{SZ}$  (Fig. 5b), where TRC eject surfzone vorticity onto the inner shelf (Fig. 4). For both models,  $S_{\omega\omega}(k_y)$  is estimated with standard techniques over 6–12 h. The funwaveC and R2  $S_{\omega\omega}(k_y)$  overall agree well. At low  $k_y$  ( $< 10^{-2} \text{ m}^{-1}$ ) both funwaveC and R2  $S_{\omega\omega}(k_y)$  are white with similar magnitudes. At  $k_y = 0.01$  to  $0.1 \text{ m}^{-1}$ ,  $S_{\omega\omega}$  rolls off similarly in both models. At larger  $k_y$  ( $> 10^{-1} \text{ m}^{-1}$ ), funwaveC and R2  $S_{\omega\omega}$  differ, but this contribution to vorticity is negligible. Because of differences in bottom stress and lateral mixing formulations, small differences in funwaveC and R2  $RMS(\omega)$  and  $S_{\omega\omega}(k_y)$  are expected, particularly at larger  $k_y$ . The similar funwaveC and R2 vorticity statistics suggest that the aliased rotational wave forcing is generating surfzone vorticity appropriately and that the funwaveC and COAWST coupling method for surfzone eddy generation works well. This gives confidence that the coupled model can be used to study 3D TRC effects on the inner shelf.

#### 4. Results: Effect of transient rip currents

Here, simulations R1 and R2 are analyzed to examine the changes that surfzone-generated TRCs induce in inner-shelf mean Lagrangian flow  $\bar{u}_L$ , eddy velocity variability, and vertical eddy diffusivity.

##### a. Effect of transient rip currents: Mean Lagrangian circulation

A Lagrangian streamfunction  $\psi_L$  is defined so that  $\bar{u}_L = -\partial\psi_L/\partial z$  and  $\bar{w}_L = \partial\psi_L/\partial x$ . Note that cross-shore gradients of  $\bar{u}_{st}$  also force mean Eulerian vertical velocity  $\bar{w}_e$ , analogous to Ekman pumping, which is also the Lagrangian velocity ( $\bar{w}_L = \bar{w}_e$ ). The  $\psi_L$  is derived from  $\bar{u}_L$  (alongshore and 12–24-h average) and is examined to elucidate the effect of transient rip currents on unstratified, inner-shelf Lagrangian circulation.

Within and immediately seaward, the surfzone ( $x \geq -1.5L_{SZ}$ , where surfzone width  $L_{SZ} = 100$  m) R1 has an overturning circulation (mostly closed  $\psi_L$  streamlines) with onshore near-surface and offshore

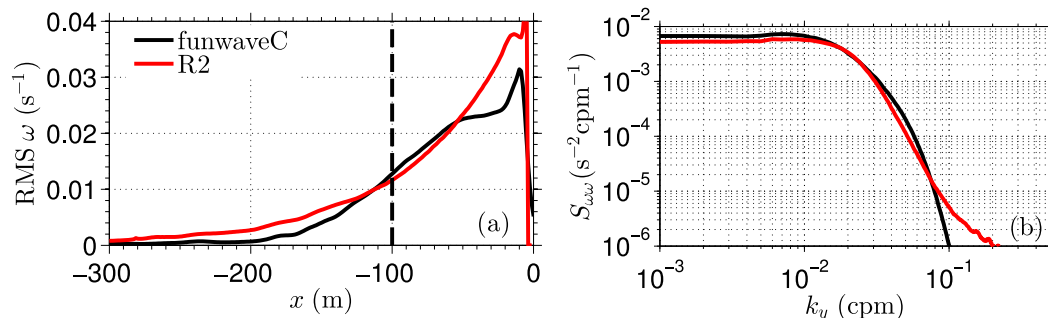


FIG. 5. (a) Root-mean-square vertical vorticity  $\omega$  simulated by funwaveC (black) and R2 (red). COAWST depth-averaged velocities are used to calculate  $\omega$ . The dashed line delimits the surfzone  $x = -L_{SZ}$ . (b) Vorticity spectra  $S_{\omega\omega}$  at  $x = -L_{SZ}$  from funwaveC (black) and R2 (red). Both RMS vorticity and vorticity spectra are estimated from over 6–12 h when the inner-shelf vorticity has equilibrated.

directed near-bottom flow as large as  $\bar{u}_L = 0.1 \text{ m s}^{-1}$  (Fig. 6a). This surfzone overturning circulation pattern is consistent with field-measured (e.g., Garcez Faria et al. 2000; Reniers et al. 2004b) and realistic modeled (Kumar et al. 2012) mean Eulerian velocity  $\bar{u}_e(x, z)$ . Not all surfzone circulation cell streamlines are closed, resulting in weak net exchange with the inner shelf (Fig. 6a). In the region from  $x = -2L_{SZ}$  to  $-6L_{SZ}$  (Fig. 6a), the  $\psi_L$  pattern indicates a weak (max  $|\bar{u}_L| = 0.002 \text{ m s}^{-1}$ ), two-layered circulation cell with upper-layer ( $z > -h/2$ ) onshore flow and lower-layer ( $z < -h/2$ ) offshore flow. Overall, the Lagrangian flow  $\bar{u}_L$  is much weaker than the nearly in balance  $\bar{u}_{st}$  or  $\bar{u}_e$ .

Transient rip currents, resulting from surfzone eddies, have a strong effect on the mean Lagrangian circulation out to  $x = -4L_{SZ}$ . In the near-surfzone region ( $x \geq -1.5L_{SZ}$ ), the R2  $\psi_L$  overturning circulation cell is similar to R1 (Fig. 6b). In contrast to R1, nearly all

surfzone-origin streamlines are closed by  $x = -2L_{SZ}$  with significant nonzero  $\bar{w}_L$ . This implies  $\bar{u}_L(z) \approx 0$  over depth at  $x \approx -2L_{SZ}$  and reduced, inner-shelf, mean, circulation-induced exchange relative to R1 (Fig. 6). Farther offshore ( $-6L_{SZ} < x < -3L_{SZ}$ ), a second overturning circulation is present, in contrast to R1, with upper-water column onshore flow, downward velocity at  $x = -3L_{SZ}$ , and offshore flow in the lower water column. (Fig. 6b). The TRC-induced differences in the mean circulation dynamics and exchange due to the mean is discussed in sections 5a and 5b, respectively.

#### b. Effect of transient rip currents: Velocity variability

The effect of surfzone-generated TRCs on the unstratified, inner-shelf velocity variability is quantified with Eulerian cross-shore and vertical velocity standard deviation [ $\sigma_u(x, z)$  and  $\sigma_w(x, z)$ ]. The R1 (no TRCs) simulation is essentially steady (Fig. 6a), and  $\sigma_u$

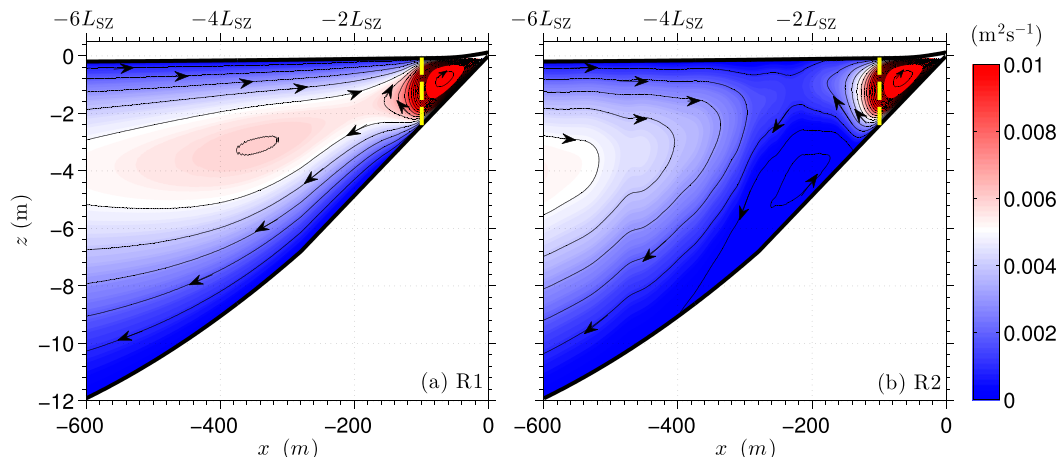


FIG. 6. (a) R1 (no TRCs) and (b) R2 (with TRCs) Lagrangian overturning streamfunction  $\psi_L$  (colors and contours at  $10^{-3} \text{ m}^2 \text{ s}^{-1}$  intervals). Arrows on the contours indicate the direction of the mean Lagrangian velocity, that is,  $\bar{u}_L = -\partial\psi_L/\partial z$  and  $\bar{w}_L = \partial\psi_L/\partial x$ . The averaging is over 12–24 h and the alongshore direction. The dashed vertical yellow line delimits the surfzone  $x = -L_{SZ}$ .

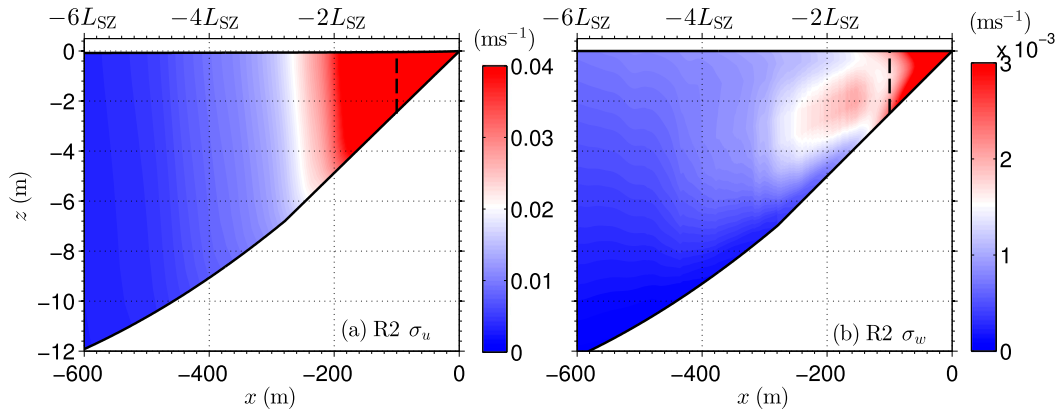


FIG. 7. R2-simulated (with TRCs) (a) cross-shore  $\sigma_u$  and (b) vertical  $\sigma_w$  Eulerian velocity standard deviation (colored). The averaging is over 12–24 h and the alongshore direction. Dashed black line delimits the surfzone  $x = -L_{SZ}$ . Note that the R1  $\sigma_u$  and  $\sigma_w$  are negligible and not shown.

and  $\sigma_w$  are negligible. Thus, the focus here is on R2, where TRCs generate inner-shelf variability (Fig. 4) and  $\sigma_u(x, z)$  and  $\sigma_w(x, z)$  are averaged over 12–24 h, and the alongshore direction. Within the surfzone ( $x > -L_{SZ}$ ) the vertically uniform  $\sigma_u \approx 0.10 \text{ m s}^{-1}$  is maximum (Fig. 7a). Farther offshore  $\sigma_u$  decreases, consistent with offshore  $\text{RMS}(\omega)$  decrease (Fig. 5a). At  $x = -2L_{SZ}$ , surface  $\sigma_u \approx 0.03 \text{ m s}^{-1}$ , and farther offshore at  $x = -3L_{SZ}$  (and  $x = -4L_{SZ}$ ), the  $\sigma_u \approx 0.014 \text{ m s}^{-1}$  ( $\sigma_u \approx 0.01 \text{ m s}^{-1}$ ). From  $-4L_{SZ} < x < -2L_{SZ}$ ,  $\sigma_u$  is about an order of magnitude stronger than  $\bar{u}_L$  (Fig. 6), suggesting that TRCs have an important role in unstratified, cross-shelf material exchange. Over this same region ( $-4L_{SZ} < x < -2L_{SZ}$ ), the top to bottom vertical variation in  $\sigma_u$  is about 20%, indicating weak, but not negligible, vertical shear in the eddies on an unstratified inner shelf (Fig. 7a). These

eddies also induce significant vertical velocities on an unstratified inner shelf. From  $x = -4L_{SZ}$  to  $x = -L_{SZ}$ , the R2 midwater column  $\sigma_w$  maxima is  $0.5\text{--}2 \times 10^{-3} \text{ m s}^{-1}$  (Fig. 7b), which are all  $\geq |\bar{u}_L|$ . These vertical velocities result from cyclostrophically balanced horizontal eddies (e.g., Burgers 1948; Rott 1958; Sullivan 1959). Beyond  $x < -5L_{SZ}$  (or  $h > 10 \text{ m}$ ),  $\sigma_u$  and  $\sigma_w$  are negligible similar to R1.

c. Effect of transient rip currents: Mean vertical eddy viscosity

The ROMS vertical eddy viscosity  $K_v$  represents the effect of turbulence on vertical momentum mixing. In both R1 and R2, surfzone turbulence  $k$  is principally generated from depth-limited, wave-breaking surface turbulence injection (e.g., Feddersen and Trowbridge 2005; Feddersen 2012). Transient rip currents export

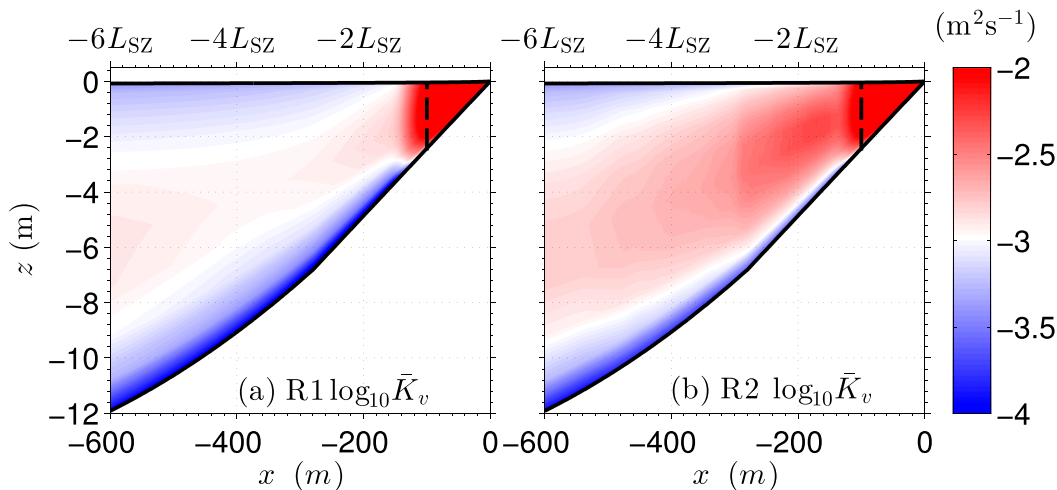


FIG. 8. (a) R1 (no TRCs) and (b) R2 (with TRCs) mean vertical eddy viscosity  $\bar{K}_v$  (colored). The averaging is over 12–24 h and the alongshore direction. Dashed black line delimits the surfzone  $x = -L_{SZ}$ .

elevated surfzone  $k$  and, as  $K_v \propto k^{1/2}$ , elevated  $K_v$  onto the inner shelf. The role of surfzone-generated TRCs in modifying unstratified inner-shelf turbulence is examined with the mean eddy viscosity  $\bar{K}_v$  (12–24-h time average and alongshore average) from R1 and R2 (Fig. 8).

In both R1 and R2, the surfzone ( $x > -L_{SZ}$ )  $\bar{K}_v$  is maximum at  $\approx 2 \times 10^{-2} \text{ m}^2 \text{ s}^{-1}$  (Fig. 8). Farther offshore ( $x = -2L_{SZ}$ ), the R1  $\bar{K}_v$  is substantially reduced with midwater column maxima near  $\approx 10^{-3} \text{ m}^2 \text{ s}^{-1}$ , decreasing to the surface and the bed (Fig. 8a) because of the reduced turbulence length scale near boundaries. This offshore diffusivity is due to the vertical shear of the Eulerian velocity (which is larger than the small Lagrangian velocities). In contrast, the R2  $\bar{K}_v$  at  $x = -2L_{SZ}$  has a midwater column maximum  $10^{-2} \text{ m}^2 \text{ s}^{-1}$  (Fig. 8b), with the entire water column significantly elevated over R1, as TRCs deliver surfzone turbulence onto the unstratified inner shelf. The R2  $\bar{K}_v$  decreases farther offshore, but even out to  $x = -4L_{SZ}$  is elevated relative to R1 (Fig. 8b), indicating that TRCs can impact unstratified water column mixing more than four surfzone widths from the shoreline. ROMS vertical eddy diffusivity (for tracers) has similar features (not shown here).

## 5. Discussion

R2 and funwaveC have statistically similar eddy fields that are also qualitatively similar to surfzone and inner-shelf eddy observations (Marmorino et al. 2013; Hally-Rosendahl et al. 2014, 2015). TRCs, generated in the surfzone, strongly impact the mean circulation, velocity variability, and turbulence on the inner shelf out to  $4L_{SZ}$  from the shoreline. Thus, the inclusion of TRC effects likely has significant impacts on the inner-shelf cross-shore sediment, pollutant, heat, larval, and nutrient fluxes. The role of (surfzone eddy generated) TRCs in modifying the inner-shelf mean circulation dynamics and a cross-shelf exchange velocity (related to flux) are considered next.

### a. Effect of transient rip currents: Mean cross-shore momentum balance

Here, the effect of TRCs on the mean, cross-shore momentum dynamics is examined at two locations. The first is  $x = -6L_{SZ}$  ( $h = 12 \text{ m}$ ), a cross-shore location far enough offshore where TRC effects on eddy velocities ( $\sigma_u$  and  $\sigma_w$ ), mean vertical eddy viscosity  $\bar{K}_v$ , and the mean Lagrangian circulation  $\psi_L$  were negligible (Figs. 6–8). The second location is at  $x = -3L_{SZ}$  ( $h = 7.4 \text{ m}$ ), where TRC effects on eddy velocities,  $\bar{K}_v$ , and  $\psi_L$  are present. In particular, at  $x = -3L_{SZ}$  the inclusion of TRCs has almost shut down the cross-shore mean

Lagrangian circulation (Fig. 6b). Mean (represented by  $\langle \cdot \rangle$ ) momentum dynamics terms are estimated by an along-shore average and 19–24-h simulation time average. Two terms are examined in detail. The first is the mean horizontal momentum advection (denoted HA):

$$\text{HA} = -\frac{\partial \langle u_e^2 \rangle}{\partial x}, \quad (9)$$

where  $u_e$  is the Eulerian velocity made up of mean and eddy contributions  $u_e = \bar{u}_e + u'_e$ . The second is the mean vertical mixing (denoted VM):

$$\text{VM} = \frac{\partial}{\partial z} \left\langle K_v \frac{\partial u_e}{\partial z} \right\rangle. \quad (10)$$

At  $x = -6L_{SZ}$  ( $h = 12 \text{ m}$ ), both R1 and R2 are in an expected, largely Stokes–Coriolis balance  $f\bar{u}_e(z) = -f\bar{u}_{st}(z)$  over most of the water column, with very small other cross-shore momentum terms (not shown). This balance is expected given that the mean  $|\bar{u}_L|$  is weak (for  $R1 \leq 0.002 \text{ m s}^{-1}$ ) offshore of  $x = -2L_{SZ}$ , the wind stress is zero, vertical mixing is relatively weak, and sufficient time has passed for adjustment. It is also consistent with observations (e.g., Lentz et al. 2008). The similar R1 and R2 dynamics at  $x = -6L_{SZ}$  explain why their mean Lagrangian overturning circulation is weak and similar (Fig. 6).

However, at  $x = -3L_{SZ}$  ( $h = 7.4 \text{ m}$ ), TRCs induce significant differences in the R1 and R2 mean cross-shore momentum balances. At  $x = -3L_{SZ}$ , the R1 (no TRCs) water column tends toward a Stokes–Coriolis balance (alongshore momentum,  $f\bar{u}_e \approx -f\bar{u}_{st}$ , with magnitude  $\approx 10^{-6} \text{ m s}^{-2}$ ) as suggested by Lentz et al. (2008) for weak vertical mixing. In the cross-shore momentum balance, a weak barotropic cross-shore pressure gradient (not shown) is balanced by weak horizontal advection ( $|\text{HA}| < 0.5 \times 10^{-6} \text{ m s}^{-2}$ ) and weaker vertical mixing ( $|\text{VM}| < 10^{-7} \text{ m s}^{-2}$ ) over the water column (Fig. 9). In contrast, the R2 (with TRCs) cross-shore momentum terms at  $x = -3L_{SZ}$  are much larger than R1 (Fig. 9), and no Stokes–Coriolis balance exists. The R2 horizontal advection  $\text{HA} \approx -3.5 \times 10^{-6} \text{ m s}^{-2}$  (Fig. 9, black dashed), much larger than R1, and reflects the offshore mean momentum flux by TRC-induced inner-shelf eddies. The R2 vertical mixing VM has a magnitude  $2 \times 10^{-6} \text{ m s}^{-2}$  (Fig. 9, red dashed), is also much larger than R1, and changes sign midwater column. Both HA and VM largely balance a cross-shore pressure gradient (not shown). The fundamentally different dynamical regime between R1 and R2 at  $x = -3L_{SZ}$  explains the dramatic differences between mean Lagrangian overturning circulation and demonstrates

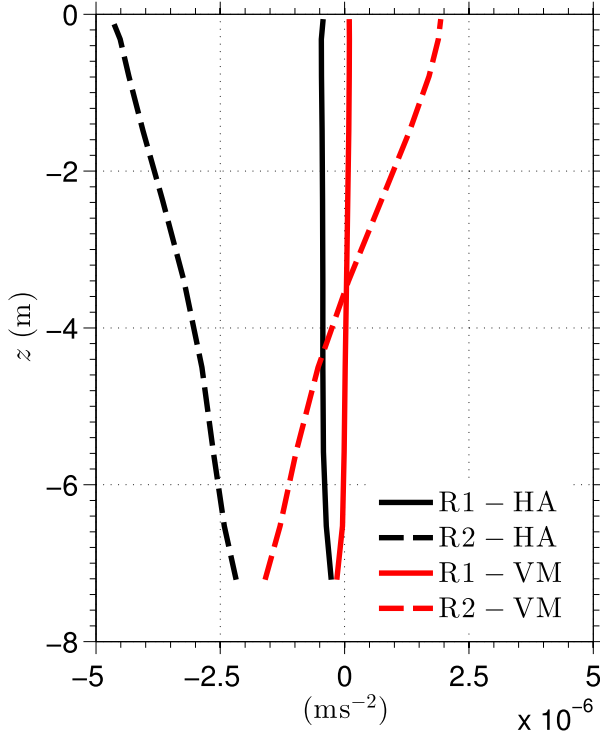


FIG. 9. R1 (solid; no TRCs) and R2 (dashed; with TRCs) mean cross-shore momentum balance terms (HA and VM) at  $x = -3L_{SZ}$ . HA (black) represents horizontal momentum advection  $-\partial\langle u_e^2 \rangle / \partial x$  that includes both Eulerian mean and eddy contributions ( $u_e = \bar{u}_e + u'_e$ ). VM (red) represents vertical mixing terms  $\partial\langle K_v \partial u_e / \partial z \rangle \partial z$ . The averaging is over 19–24 h and the alongshore direction.

the effects that TRCs can have on the mean overturning circulation. Between  $-6L_{SZ} < x < -3L_{SZ}$  the R2 mean cross-shore momentum dynamics transition from eddy-dominated to Stokes–Coriolis-dominated regimes.

#### b. Effect of transient rip currents: Cross-shore exchange velocity

On alongshore, uniform beaches, both transient rip currents (Hally-Rosendahl et al. 2015; Suanda and Feddersen 2015) and vertical mismatch between Stokes drift velocity and the return Eulerian-mean flow (e.g., Lentz et al. 2008; Kumar et al. 2012) are potential cross-shore exchange mechanisms across the inner shelf. Their relative importance in driving exchange across the inner shelf is not understood. Here, surfzone-generated TRC (R2) significantly impacted the inner-shelf velocities and mixing  $4L_{SZ}$  from the shoreline (Figs. 6–8). Here, the R1 and R2 cross-shelf exchange is quantified with an exchange velocity  $U_{ex}$ , defined as

$$U_{ex}(x) = \left\langle \frac{-1}{(h + \eta)} \int_{-h}^{\eta} u_L^-(x, y, z, t) dz \right\rangle, \quad (11)$$

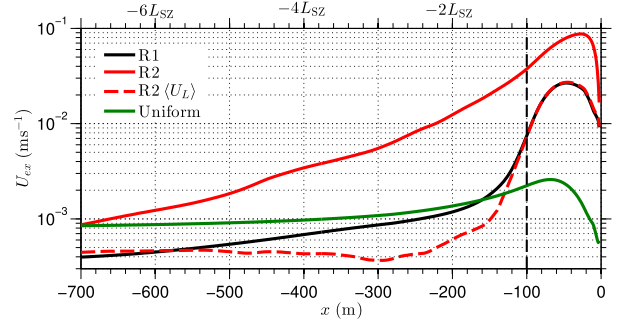


FIG. 10. Exchange velocity  $U_{ex}$  (11) for unstratified simulations R1 (black; no TRCs), R2 (red; with TRCs), and  $\bar{u}_L$ -derived R2 (red dashed). In addition,  $U_{ex}$  assuming uniform Eulerian return flow balancing onshore Stokes drift (Hally-Rosendahl et al. 2014) is shown (green). Dashed black line delimits the surfzone  $x = -L_{SZ}$ .

where  $u_L^-$  is the instantaneous offshore directed  $u_L$  (and is zero for onshore  $u_L$ ),  $\eta$  is the sea surface elevation, and  $\langle \cdot \rangle$  represents an average over 12–24 h and the alongshore direction. This exchange velocity  $U_{ex}$  [(11)] is analogous to the estuarine total exchange flow (MacCready 2011) and is a 3D version of the two-dimensional rip-current exchange velocity (Suanda and Feddersen 2015). Here, the cross-shore variation of exchange velocity  $U_{ex}(x)$  is examined for R1 and R2 (Fig. 10) to highlight the effect of TRCs on cross-shelf exchange. To isolate the effects of the mean Lagrangian circulation (Fig. 6), an additional R2  $U_{ex}$  is calculated using only the offshore-directed mean Lagrangian velocity  $\bar{u}_L^-$  in (11).

For R1 (no TRCs), the vertical mismatch between Stokes drift  $\bar{u}_{st}$  and return Eulerian flow  $\bar{u}_e$  result in an overturning mean Lagrangian circulation (Fig. 6a) and a nonzero cross-shelf exchange velocity  $U_{ex}^{(R1)}$  (solid black line, Fig. 10). Maximum  $U_{ex}^{(R1)} = 0.025 \text{ m s}^{-1}$  occurs midsurfzone, corresponding to the strong surfzone overturning circulation (Fig. 6a), and decreases rapidly to  $U_{ex}^{(R1)} = 0.002 \text{ m s}^{-1}$  at  $x = -5L_{SZ}$ . Farther offshore,  $U_{ex}^{(R1)}$  decreases more slowly to  $U_{ex}^{(R1)} = 4 \times 10^{-4} \text{ m s}^{-1}$  at  $x = -6L_{SZ}$  (Fig. 10). The  $U_{ex}^{(R1)}$  represents the exchange induced only by the Stokes drift. A Stokes drift-driven exchange velocity  $U_{ex}^{(st)}$  has been analytically estimated, assuming a depth-uniform Eulerian return flow balancing the onshore Stokes drift mass flux (e.g., Hally-Rosendahl et al. 2014; Suanda and Feddersen 2015). In the inner-shelf region from  $-4L_{SZ} < x < -1.5L_{SZ}$ , this  $U_{ex}^{(st)} \approx 10^{-3} \text{ m s}^{-1}$  is comparable to or slightly larger than  $U_{ex}^{(R1)}$  (cf. green and black, Fig. 10), indicating that  $U_{ex}^{(st)}$  reasonably estimates Stokes drift-driven exchange in this inner-shelf region, even though the  $\bar{u}_e$  is not depth uniform (e.g., Lentz et al. 2008). At  $x = -3L_{SZ}$ ,  $U_{ex}^{(st)}$  overestimates  $U_{ex}^{(R1)}$  as R1 is near a Stokes–Coriolis

balance with very weak,  $\bar{u}_L \approx 0$  and  $U_{\text{ex}}^{(\text{st})}$  assumes a depth-uniform return flow.

For R2 (with TRCs), both the overturning circulation (Fig. 6b) and inner-shelf TRC-induced eddies (Fig. 4) contribute to cross-shelf exchange. Surfzone  $U_{\text{ex}}^{(\text{R2})}$  varies from 0.04 to 0.09  $\text{m s}^{-1}$  (solid red, Fig. 10) and is significantly larger than the surfzone  $U_{\text{ex}}^{(\text{R1})}$ , indicating that eddies and not undertow dominate cross-surfzone exchange (e.g., Clark et al. 2010). On the inner shelf at  $x = -2L_{\text{SZ}}$ ,  $U_{\text{ex}}^{(\text{R2})} \approx 10^{-2} \text{m s}^{-1}$ , an order of magnitude larger than  $U_{\text{ex}}^{(\text{R1})} \approx 10^{-3} \text{m s}^{-1}$  (Fig. 10), and is consistent with the temperature- and dye-inferred exchange velocity with similar wave conditions (Hally-Rosendahl et al. 2014, 2015). Across the model domain,  $U_{\text{ex}}^{(\text{R2})}$  is consistently larger than  $U_{\text{ex}}^{(\text{R1})}$ . Even at  $x = -5L_{\text{SZ}}$ , the  $U_{\text{ex}}^{(\text{R2})}$  is 3 times the  $U_{\text{ex}}^{(\text{R1})}$ . On the inner-shelf  $U_{\text{ex}}^{(\text{R2})}$  decays exponentially and less rapidly than the parameterized  $U_{\text{ex}}$  decay based on depth-integrated funwaveC simulations (Suanda and Feddersen 2015), potentially due to 3D effects. Across the inner shelf, the eddy contribution to  $U_{\text{ex}}^{(\text{R2})}$  dominates over the mean circulation exchange contributions (cf. solid and dashed red curves). Even at  $x = -5L_{\text{SZ}}$  ( $h = 11.2 \text{m}$ ),  $U_{\text{ex}}^{(\text{R2})} \approx 3U_{\text{ex}}^{(\text{R1})}$ . Consistent with the weaker R2 (relative to R1) Lagrangian overturning circulation (Fig. 6), the R2  $\bar{u}_L$ -derived  $U_{\text{ex}}$  is weaker than  $U_{\text{ex}}^{(\text{R1})}$  from  $-5L_{\text{SZ}} < x < -1.5L_{\text{SZ}}$  (cf. red dashed and black curves, Fig. 10). This demonstrates the importance of transient rip currents to cross-shore exchange on the inner shelf.

### c. Neglecting current effects on waves

These simulations (R1 and R2) and those of Part II do not include the effect of currents on surface gravity waves [current effect on waves (CEW)] such as current-induced refraction. CEW effects were also neglected in other realistic, depth-integrated and wave-averaged (e.g., Reniers et al. 2004a; Long and Özkan-Haller 2005, 2009) and depth-resolving and wave-averaged (e.g., Reniers et al. 2004b; Uchiyama et al. 2010) nearshore circulation studies. CEW effects become important when the cross-shore Eulerian velocity is significant relative to the wave speed  $c = (gh)^{1/2}$ , as in depth-integrated and wave-averaged modeling studies of shear instabilities and bathymetrically controlled rip currents that included CEW (Haas et al. 1998; Yu and Slinn 2003; Özkan-Haller and Li 2003; Uchiyama et al. 2009; Kumar et al. 2012). For R2 at the surfzone boundary  $x = -L_{\text{SZ}}$  and  $h = 2.5 \text{m}$ , resulting in  $c = 5 \text{m s}^{-1}$  and  $\sigma_u = 0.1 \text{m s}^{-1}$  (Fig. 7). Thus,  $\sigma_u/c = 0.02$  is very small and decays farther offshore. The maximum  $\sigma_u/c = 0.10$  occurs farther onshore in the inner surfzone at  $x = -0.24L_{\text{SZ}}$ . Furthermore, at  $x = -L_{\text{SZ}}$ , the

R2 vorticity statistics were similar to funwaveC (which intrinsically includes CEW), which indicates that neglecting CEW is appropriate here.

## 6. Summary

Transient rip currents (TRCs) must be accurately simulated to understand cross-shore exchange, stratification evolution, and mixing on the inner shelf. In this two-part study, a depth-integrated, wave-resolving, Boussinesq model funwaveC is coupled to a 3D, wave-averaged ocean circulation and wave propagation model COAWST and used to diagnose Stokes drift and TRC effects on an unstratified inner shelf (this work, Part I) and, in Part II, a stratified inner shelf. Here, the funwaveC and COAWST coupling methodology is developed to allow surfzone eddy forcing and TRC generation in COAWST. Two, nearly identical, unstratified, vertically resolving COAWST simulations are performed without TRC effect (simulation R1, no funwaveC coupling) and with TRC effects (simulation R2). The R2 and funwaveC vertical vorticity (i.e., eddy) statistics are similar, indicating the model coupling is accurately generating TRCs.

The R1 and R2 inner-shelf mean Lagrangian velocities are weak. The R1 (no TRCs) inner-shelf mean Lagrangian circulation has a weak clockwise overturning circulation cell with near-surface onshore flow and near-bed offshore flow. R2 (with TRCs) has a surfzone clockwise Lagrangian circulation cell and a largely separate offshore ( $x < -3L_{\text{SZ}}$ , where  $L_{\text{SZ}}$  is the surfzone width) clockwise cell with very few streamlines connecting the two. The R2 inner-shelf cross-shore and vertical velocity variability are stronger than the mean Lagrangian flow, are maximum near the surfzone, and decay offshore to being negligible at  $x = -4L_{\text{SZ}}$ . The cross-shore velocities are largely depth-uniform, and vertical velocities are maximum in midwater column. The R2 inner-shelf mean vertical eddy diffusivity is an order of magnitude larger than R1 as TRCs enhance unstratified, inner-shelf turbulence.

At  $x = -6L_{\text{SZ}}$ , R1 and R2 momentum dynamics indicate a Stokes–Coriolis balance, as expected for no wind stress and negligible vertical mixing. At  $x = -3L_{\text{SZ}}$ , R1 momentum dynamics tend to a Stokes–Coriolis balance. In contrast at  $x = -3L_{\text{SZ}}$ , R2 horizontal advection and vertical mixing induced by TRCs balance the cross-shore pressure gradient. The R2 exchange velocity is 2 to 10 times larger than for R1 out to  $x = -5L_{\text{SZ}}$ , indicating that TRCs are the dominant exchange mechanism in this region. Within  $4L_{\text{SZ}}$  of the shoreline, unstratified, inner-shelf simulations of pollution, larval, or sediment transport should include

transient rip currents. In Part II, the effects of Stokes drift and TRCs on the stratified inner shelf are examined.

*Acknowledgments.* Support for N. Kumar and F. Feddersen was provided by the Office of Naval Research (ONR) Grant N00014-14-1-0553. Computational support was provided by the COMPAS/ATLAS cluster maintained by Caroline Papadopoulos and Bruce Cornuelle. K. Winters, S. H. Suanda, P. MacCready, and M. S. Spydell provided useful feedback.

## REFERENCES

- Allen, J., P. Newberger, and J. Federiuk, 1995: Upwelling circulation on the Oregon continental shelf. Part I: Response to idealized forcing. *J. Phys. Oceanogr.*, **25**, 1843–1866, doi:10.1175/1520-0485(1995)025<1843:UCOTOC>2.0.CO;2.
- Austin, J. A., and S. J. Lentz, 2002: The inner shelf response to wind-driven upwelling and downwelling. *J. Phys. Oceanogr.*, **32**, 2171–2193, doi:10.1175/1520-0485(2002)032<2171:TISRTRW>2.0.CO;2.
- Boehm, A. B., N. S. Ismail, L. M. Sassoubre, and E. A. Andruszkiewicz, 2017: Oceans in peril: Grand challenges in applied water quality research for the 21st century. *Environ. Eng. Sci.*, **34**, 3–15, doi:10.1089/ees.2015.0252.
- Booij, N., R. Ris, and L. H. Holthuisen, 1999: A third-generation wave model for coastal regions: 1. Model description and validation. *J. Geophys. Res.*, **104**, 7649–7666, doi:10.1029/98JC02622.
- Brown, J. A., J. H. MacMahan, A. J. H. M. Reniers, and E. B. Thornton, 2015: Field observations of surf zone–inner shelf exchange on a rip-channeled beach. *J. Phys. Oceanogr.*, **45**, 2339–2355, doi:10.1175/JPO-D-14-0118.1.
- Burgers, J. M., 1948: A mathematical model illustrating the theory of turbulence. *Adv. Appl. Mech.*, **1**, 171–199, doi:10.1016/S0065-2156(08)70100-5.
- Clark, D. B., F. Feddersen, and R. T. Guza, 2010: Cross-shore surfzone tracer dispersion in an alongshore current. *J. Geophys. Res.*, **115**, C10035, doi:10.1029/2009JC005683.
- , —, and —, 2011: Modeling surfzone tracer plumes: 2. Transport and dispersion. *J. Geophys. Res.*, **116**, C11028, doi:10.1029/2011JC007211.
- , S. Elgar, and B. Raubenheimer, 2012: Vorticity generation by short-crested wave breaking. *Geophys. Res. Lett.*, **39**, L24604, doi:10.1029/2012GL054034.
- Craik, A., and S. Leibovich, 1976: A rational model for Langmuir circulations. *J. Fluid Mech.*, **73**, 401–426, doi:10.1017/S0022112076001420.
- Dalrymple, R. A., J. H. MacMahan, A. J. Reniers, and V. Nelko, 2011: Rip currents. *Annu. Rev. Fluid Mech.*, **43**, 551–581, doi:10.1146/annurev-fluid-122109-160733.
- Feddersen, F., 2012: Scaling surfzone turbulence. *Geophys. Res. Lett.*, **39**, L18613, doi:10.1029/2012GL052970.
- , 2014: The generation of surfzone eddies in a strong alongshore current. *J. Phys. Oceanogr.*, **44**, 600–617, doi:10.1175/JPO-D-13-051.1.
- , and J. H. Trowbridge, 2005: The effect of wave breaking on surf-zone turbulence and alongshore currents: A modelling study. *J. Phys. Oceanogr.*, **35**, 2187–2204, doi:10.1175/JPO2800.1.
- , D. B. Clark, and R. T. Guza, 2011: Modeling of surf zone tracer plumes: 1. Waves, mean currents, and low-frequency eddies. *J. Geophys. Res.*, **116**, C11027, doi:10.1029/2011JC007210.
- , M. Olabarrieta, R. T. Guza, D. Winters, B. Raubenheimer, and S. Elgar, 2016: Observations and modeling of a tidal inlet dye tracer plume. *J. Geophys. Res. Oceans*, **121**, 7819–7844, doi:10.1002/2016JC0011922.
- Fewings, M., S. J. Lentz, and J. Fredericks, 2008: Observations of cross-shelf flow driven by cross-shelf winds on the inner continental shelf. *J. Phys. Oceanogr.*, **38**, 2358–2378, doi:10.1175/2008JPO3990.1.
- Fujimura, A., A. Reniers, C. C. Paris, A. L. Shanks, J. MacMahan, and S. Morgan, 2014: Numerical simulations of larval transport into a rip-channeled surf zone. *Limnol. Oceanogr.*, **59**, 1434–1447, doi:10.4319/lo.2014.59.4.1434.
- Garcez Faria, A., E. Thornton, T. Lippmann, and T. Stanton, 2000: Undertow over a barred beach. *J. Geophys. Res.*, **105**, 16 999–17 010, doi:10.1029/2000JC900084.
- Guza, R. T., and F. Feddersen, 2012: Effect of wave frequency and directional spread on shoreline runup. *Geophys. Res. Lett.*, **39**, L11607, doi:10.1029/2012GL051959.
- Haas, K. A., I. A. Svensen, and M. C. Haller, 1998: Numerical modeling of nearshore circulation on a barred beach with rip currents. *Proc. 26th Conf. on Coastal Engineering*, Copenhagen, Denmark, ASCE, 801–814.
- Haidvogel, and Coauthors, 2008: Ocean forecasting in terrain-following coordinates: Formulation and skill assessment of the regional ocean modeling system. *J. Comput. Phys.*, **227**, 3595–3624, doi:10.1016/j.jcp.2007.06.016.
- Haines, J. W., and A. H. Sallenger, 1994: Vertical structure of mean cross-shore currents across a barred surf zone. *J. Geophys. Res.*, **99**, 14 223–14 242, doi:10.1029/94JC00427.
- Hally-Rosendahl, K., and F. Feddersen, 2016: Modeling surfzone to inner-shelf tracer exchange. *J. Geophys. Res. Oceans*, **121**, 4007–4025, doi:10.1002/2015JC011530.
- , —, and R. T. Guza, 2014: Cross-shore tracer exchange between the surfzone and inner-shelf. *J. Geophys. Res. Oceans*, **119**, 4367–4388, doi:10.1002/2013JC009722.
- , —, D. B. Clark, and R. Guza, 2015: Surfzone to inner-shelf exchange estimated from dye tracer balances. *J. Geophys. Res. Oceans*, **120**, 6289–6308, doi:10.1002/2015JC010844.
- Halpern, B. S., and Coauthors, 2008: A global map of human impact on marine ecosystems. *Science*, **319**, 948–952, doi:10.1126/science.1149345.
- Horwitz, R., and S. J. Lentz, 2014: Inner-shelf response to cross-shelf wind stress: The importance of the cross-shelf density gradient in an idealized numerical model and field observations. *J. Phys. Oceanogr.*, **44**, 86–103, doi:10.1175/JPO-D-13-075.1.
- Johnson, D., and C. Pattiaratchi, 2006: Boussinesq modelling of transient rip currents. *Coastal Eng.*, **53**, 419–439, doi:10.1016/j.coastaleng.2005.11.005.
- Kennedy, A. B., Q. H. Chen, J. T. Kirby, and R. A. Dalrymple, 2000: Boussinesq modeling of wave transformation, breaking and runup. I: 1D. *J. Waterw. Port Coastal Ocean Eng.*, **126**, 39–47, doi:10.1061/(ASCE)0733-950X(2000)126:1(39).
- Kirincich, A. R., J. A. Barth, B. A. Grantham, B. A. Menge, and J. Lubchenco, 2005: Wind-driven inner-shelf circulation off central Oregon during summer. *J. Geophys. Res.*, **110**, C10S03, doi:10.1029/2004JC002611.
- , S. J. Lentz, and J. A. Barth, 2009: Wave-driven inner-shelf motions on the Oregon coast. *J. Phys. Oceanogr.*, **39**, 2942–2956, doi:10.1175/2009JPO4041.1.

- Kumar, N., and F. Feddersen, 2016: The effect of Stokes drift and transient rip currents on the inner shelf. Part II: With stratification. *J. Phys. Oceanogr.*, **47**, 243–260, doi:10.1175/JPO-D-16-0077.1.
- , G. Voulgaris, and J. C. Warner, 2011: Implementation and modification of a three-dimensional radiation stress formulation for surf zone and rip-current applications. *Coastal Eng.*, **58**, 1097–1117, doi:10.1016/j.coastaleng.2011.06.009.
- , —, —, and M. Olabarrieta, 2012: Implementation of the vortex force formalism in the coupled ocean-atmosphere-wave-sediment transport (COAWST) modeling system for inner shelf and surf zone applications. *Ocean Modell.*, **47**, 65–95, doi:10.1016/j.ocemod.2012.01.003.
- , F. Feddersen, Y. Uchiyama, J. McWilliams, and W. O'Reilly, 2015: Midshelf to surfzone coupled ROMS–SWAN model data comparison of waves, currents, and temperature: Diagnosis of subtidal forcings and response. *J. Phys. Oceanogr.*, **45**, 1464–1490, doi:10.1175/JPO-D-14-0151.1.
- , —, S. Suanda, Y. Uchiyama, and J. McWilliams, 2016: Mid-to inner-shelf coupled ROMS–SWAN model–data comparison of currents and temperature: Diurnal and semi-diurnal variability. *J. Phys. Oceanogr.*, **46**, 841–862, doi:10.1175/JPO-D-15-0103.1.
- Lentz, S. J., 2001: The influence of stratification on the wind-driven cross-shelf circulation over the North Carolina shelf. *J. Phys. Oceanogr.*, **31**, 2749–2760, doi:10.1175/1520-0485(2001)031<2749:TIOSOT>2.0.CO;2.
- , and M. R. Fewings, 2012: The wind- and wave-driven inner-shelf circulation. *Annu. Rev. Mar. Sci.*, **4**, 317–343, doi:10.1146/annurev-marine-120709-142745.
- , M. Fewings, P. Howd, J. Fredericks, and K. Hathaway, 2008: Observations and a model of undertow over the inner continental shelf. *J. Phys. Oceanogr.*, **38**, 2341–2357, doi:10.1175/2008JPO3986.1.
- Long, J. W., and H. T. Özkan-Haller, 2005: Offshore controls on nearshore rip currents. *J. Geophys. Res.*, **110**, C12007, doi:10.1029/2005JC003018.
- , and —, 2009: Low-frequency characteristics of wave group–forced vortices. *J. Geophys. Res.*, **114**, C08004, doi:10.1029/2008JC004894.
- Lynett, P., 2006: Nearshore wave modeling with high-order Boussinesq-type equations. *J. Waterw. Port Coastal Ocean Eng.*, **132**, 348–357, doi:10.1061/(ASCE)0733-950X(2006)132:5(348).
- MacCready, P., 2011: Calculating estuarine exchange flow using isohaline coordinates. *J. Phys. Oceanogr.*, **41**, 1116–1124, doi:10.1175/2011JPO4517.1.
- MacMahan, J. H., E. B. Thornton, and A. J. Reniers, 2006: Rip current review. *Coastal Eng.*, **53**, 191–208, doi:10.1016/j.coastaleng.2005.10.009.
- Marmorino, G. O., G. B. Smith, and W. D. Miller, 2013: Infrared remote sensing of surf-zone eddies. *IEEE J. Sel. Top. Appl. Earth Obs. Remote Sens.*, **6**, 1710–1718, doi:10.1109/JSTARS.2013.2257695.
- McWilliams, J. C., J. M. Restrepo, and E. M. Lane, 2004: An asymptotic theory for the interaction of waves and currents in coastal waters. *J. Fluid Mech.*, **511**, 135–178, doi:10.1017/S0022112004009358.
- Nwogu, O., 1993: Alternative form of Boussinesq equations for nearshore wave propagation. *J. Waterw. Port Coastal Ocean Eng.*, **119**, 618–638, doi:10.1061/(ASCE)0733-950X(1993)119:6(618).
- Olabarrieta, M., J. C. Warner, and N. Kumar, 2011: Wave-current interaction in Willapa Bay. *J. Geophys. Res.*, **116**, C12014, doi:10.1029/2011JC007387.
- Özkan Haller, H. T., 2014: Vertical variability of undertow and longshore currents outside the surf zone. *J. Waterw. Port Coastal Ocean Eng.*, **140**, 4–13, doi:10.1061/(ASCE)WW.1943-5460.0000219.
- , and Y. Li, 2003: Effects of wave-current interaction on shear instabilities of longshore currents. *J. Geophys. Res.*, **108**, 3139, doi:10.1029/2001JC001287.
- Peregrine, D. H., 1998: Surf zone currents. *Theor. Comput. Fluid Dyn.*, **10**, 295–309, doi:10.1007/s001620050065.
- Pineda, J., J. A. Hare, and S. Sponaugle, 2007: Larval transport and dispersal in the coastal ocean and consequences for population connectivity. *Oceanography*, **20**, 22–39, doi:10.5670/oceanog.2007.27.
- Reniers, A. J. H. M., J. A. Roelvink, and E. B. Thornton, 2004a: Morphodynamic modeling of an embayed beach under wave group forcing. *J. Geophys. Res.*, **109**, C01030, doi:10.1029/2002JC001586.
- , E. Thornton, T. Stanton, and J. Roelvink, 2004b: Vertical flow structure during Sandy Duck: Observations and modeling. *Coastal Eng.*, **51**, 237–260, doi:10.1016/j.coastaleng.2004.02.001.
- , J. H. MacMahan, E. B. Thornton, T. P. Stanton, M. Henriquez, J. W. Brown, J. A. Brown, and E. Gallagher, 2009: Surf zone surface retention on a rip-channeled beach. *J. Geophys. Res.*, **114**, C10010, doi:10.1029/2008JC005153.
- Ris, R., L. Holthuijsen, and N. Booij, 1999: A third-generation wave model for coastal regions: 2. Verification. *J. Geophys. Res.*, **104**, 7667–7681, doi:10.1029/1998JC900123.
- Rott, N., 1958: On the viscous core of a line vortex. *Z. Angew. Math. Phys. ZAMP*, **9**, 543–553, doi:10.1007/BF02424773.
- Shanks, A. L., S. G. Morgan, J. MacMahan, and A. J. Reniers, 2010: Surf zone physical and morphological regime as determinants of temporal and spatial variation in larval recruitment. *J. Exp. Mar. Biol. Ecol.*, **392**, 140–150, doi:10.1016/j.jembe.2010.04.018.
- Shchepetkin, A. F., and J. C. McWilliams, 2005: The Regional Oceanic Modeling System (ROMS): A split-explicit, free-surface, topography-following-coordinate oceanic model. *Ocean Modell.*, **9**, 347–404, doi:10.1016/j.ocemod.2004.08.002.
- , and —, 2009: Correction and commentary for “Ocean forecasting in terrain-following coordinates: Formulation and skill assessment of the regional ocean modeling system” by Haidvogel and Coauthors, *J. Comp. Phys.*, **227**, pp. 3595–3624. *J. Comput. Phys.*, **228**, 8985–9000, doi:10.1016/j.jcp.2009.09.002.
- Spydell, M. S., and F. Feddersen, 2009: Lagrangian drifter dispersion in the surf zone: Directionally spread, normally incident waves. *J. Phys. Oceanogr.*, **39**, 809–830, doi:10.1175/2008JPO3892.1.
- , —, R. T. Guza, and W. E. Schmidt, 2007: Observing surf-zone dispersion with drifters. *J. Phys. Oceanogr.*, **37**, 2920–2939, doi:10.1175/2007JPO3580.1.
- , —, and —, 2009: Observations of drifter dispersion in the surfzone: The effect of sheared alongshore currents. *J. Geophys. Res.*, **114**, C07028, doi:10.1029/2009JC005328.
- Suanda, S. H., and F. Feddersen, 2015: A self-similar scaling for cross-shelf exchange driven by transient rip currents. *Geophys. Res. Lett.*, **42**, 5427–5434, doi:10.1002/2015GL063944.
- , S. Perez, and F. Feddersen, 2016: Evaluation of a source-function wavemaker for generating random directionally spread waves in the sea-swell band. *Coastal Eng.*, **114**, 220–232, doi:10.1016/j.coastaleng.2016.04.006.

- Sullivan, R. D., 1959: A two-cell vortex solution of the Navier–Stokes equations. *J. Aerosp. Sci.*, **26**, 767–768, doi:10.2514/8.8303.
- Tilburg, C., 2003: Across-shelf transport on a continental shelf: Do across-shelf winds matter? *J. Phys. Oceanogr.*, **33**, 2675–2688, doi:10.1175/1520-0485(2003)033<2675:ATOACS>2.0.CO;2.
- Uchiyama, Y., J. C. McWilliams, and J. M. Restrepo, 2009: Wave-current interaction in nearshore shear instability analyzed with a vortex force formalism. *J. Geophys. Res.*, **114**, C06021, doi:10.1029/2008JC005135.
- , —, and A. F. Shchepetkin, 2010: Wave-current interaction in an oceanic circulation model with a vortex-force formalism: Application to the surf zone. *Ocean Modell.*, **34**, 16–35, doi:10.1016/j.ocemod.2010.04.002.
- Warner, J. C., C. R. Sherwood, H. G. Arango, and R. P. Signell, 2005: Performance of four turbulence closure models implemented using a generic length scale method. *Ocean Modell.*, **8**, 81–113, doi:10.1016/j.ocemod.2003.12.003.
- , B. Armstrong, R. He, and J. B. Zambon, 2010: Development of a Coupled Ocean–Atmosphere–Wave–Sediment Transport (COAWST) modeling system. *Ocean Modell.*, **35**, 230–244, doi:10.1016/j.ocemod.2010.07.010.
- Wei, G., J. T. Kirby, and A. Sinha, 1999: Generation of waves in Boussinesq models using a source function method. *Coastal Eng.*, **36**, 271–299, doi:10.1016/S0378-3839(99)00009-5.
- Xu, Z., and A. J. Bowen, 1994: Wave- and wind-driven flow in water of finite depth. *J. Phys. Oceanogr.*, **24**, 1850–1866, doi:10.1175/1520-0485(1994)024<1850:WAWDFI>2.0.CO;2.
- Yu, J., and D. N. Slinn, 2003: Effects of wave-current interaction on rip currents. *J. Geophys. Res.*, **108**, 3088, doi:10.1029/2001JC001105.